Experimental and field study of the effects of lithological contrasts on thrust-related deformation

Antonio Teixell

Departament de Geologia, Universitat Autònoma de Barcelona, Bellaterra, Spain

Hemin A. Koyi

Hans Ramberg Tectonic Laboratory, Department of Earth Sciences, Uppsala University, Uppsala, Sweden

Received 6 May 2002; revised 12 June 2003; accepted 25 June 2003; published 15 October 2003.

[1] The influence of mechanical contrasts related to stratigraphy on thrust-related deformation are investigated by sandbox modeling using combinations of granular materials possessing different mechanical properties and by structural analysis of a natural example from the Spanish Pyrenees. The models used in this study consist of loose sand and glass microbeads, in varied stratigraphic thicknesses and sequences, and the natural example consists of a weakening-upward sequence of sandstones and carbonates. In both cases, layers of different composition had a mechanical significance and accommodated shortening differently. Model sand and natural sandstone exhibited most shortening by thrust imbrication irrespective of stratigraphic position, whereas glass microbeads and carbonates exhibited wider deformation zones and enhanced folding, accompanied by displacement reduction along thrust surfaces cutting them. Transitions of structural style were guided by the stratigraphy rather than by a simple unidirectional propagation from a step up. Layer-parallel shortening was accommodated by diverse mechanisms but did not vary significantly in layers which had different properties. The magnitude with which mechanical contrasts were expressed in the models was influenced by the strength at the décollement zone. The effect of mechanical contrast was more profound in models shortened above a low-friction décollement. *INDEX TERMS:* 8005 Structural Geology: Folds and folding; 8010 Structural Geology: Fractures and faults; 8102 Tectonophysics: Continental contractional orogenic belts; *KEYWORDS:* thrust, deformation, mechanical stratigraphy, analogue modeling, Pyrenees. **Citation:** Teixell, A., and H. A. Koyi, Experimental and field study of the effects of lithological contrasts on thrust-related deformation, *Tectonics*, *22*(5), 1054, doi:10.1029/2002TC001407, 2003.

0278-7407/03/2002TC001407$12.00

1. Introduction

[2] Geometric, analogue and numerical modeling of thrust systems have considerably improved our understanding of upper crustal deformation. [e.g., *Suppe*, 1983; *Davis et al.*, 1983; *Malavieille*, 1984; *Mulugeta and Koyi*, 1987, 1992; *Suppe and Medwedeff*, 1990; *Mitra*, 1990; *Colleta et al.*, 1991; *Liu et al.*, 1992; *Koyi*, 1995; *Hardy and Ford*, 1997; *Gutscher et al.*, 1998]. In these studies mechanically uniform layered successions are usually used. However, many natural thrust systems involve stratigraphic successions composed of layers of varied mechanical properties, which do not behave passively during deformation.

[3] Although competence contrasts are classical concepts in structural geology, their effects in thrust tectonics have comparatively received much less attention. *Morley* [1986] documented the influence of lithological variations in vertical contrasts of deformation style within a natural thrust sheet, essentially by examining the distribution of minor thrusts and the variation of fault throw across the stratigraphy. *Gross et al.* [1997] investigated displacement length relations as function of the mechanical stratigraphy in strike-parallel normal faults formed in a compressional setting. On a larger scale, *Woodward and Rutherford* [1989] argued for the mechanical significance of stratigraphic variations by studying lateral differences in thrust-related structural style (fold and fault spacing) in areas with facies changes. In a recent work, *Chester* [2003] describes an upward transition from close-spaced duplex thrusts to broad folds guided by the mechanical stratigraphy and the detachment levels. Among the few analogue models which simulate aspects of vertical mechanical variations are those of *Liu and Dixon* [1991] and *Dixon and Liu* [1992], which modeled buckling and subsequent ramp generation in alternating successions of viscous materials. *Chester et al.* [1991], used nonscaled rock models to simulate heterogeneous layering influences on fault bend and fault propagation folding. *Liu et al.* [1992] placed thin interlayers of mica flakes within frictional sandbox models to introduce anisotropy and enhance folding, and most recently, *Turrini et al.* [2001] used nontabular experimental stratigraphic prisms with interbedded sand and glass bead layers to model multiple detachment levels and ramp-flat geometries.

[4] In this work we address the effects of vertical compositional and mechanical contrasts in folding and deformation style associated with thrust tectonics. We do that by

Table 1. Model Parameters and Material Types

Model	Stratigraphy (From Top to Bottom)	Thickness, mm	Type of Décollement	% Shortening
1	glass beads; sand and beads[a]; sand	26	high friction (sand-metal base)	40
2	glass beads; sand and beads; sand	26	low friction (glass beads)	34
3	glass beads; sand	12	low friction (glass beads)	45
4	sand; glass beads	12	low friction (glass beads)	45

[a]"Sand and beads" corresponds to a 50% mixture of sand and glass microbeads.

using sandbox models consisting of combinations of different granular materials and a particularly illustrative natural example from the Spanish Pyrenees. We show that variations of mechanical properties across a succession have a profound effect on many features of thrust imbricate wedges, such as: a) strain partitioning (distribution of shortening mechanisms in the stratigraphy), b) primary thrust attitudes (fault slip, cutoff angles, etc.), c) fault-related folding style and width of fault damage zones, and ultimately, d) wedge taper evolution. Many of these variations are expressed along single faults as they cut across different units. The influence of stratigraphic variations on the fault-related folding in the Pyrenean natural example has been outlined in a previous paper by *Alonso and Teixell* [1992].

2. Sandbox Analogue Models

[5] Although deformation mechanisms at the small-scale are not conveniently simulated in sandbox experiments due to the scaling of grains, loose sand and other granular materials are appropriate to model macroscopic deformation features in upper crustal rocks dominated by frictional behavior. In order to simulate competence contrasts in upper crustal layered rocks we prepared models combining different granular materials, namely sand, glass microbeads, and a 50% mixture of the two, which display different coefficient of friction, and thus different mechanical strength (Table 1). Erosion or syntectonic sedimentation was not incorporated in the models described here. These processes, which otherwise may play a significant role in the evolution of an entire fold-thrust belt, would probably have had minor influence on the local structural development of the single thrust faults in our study. The thrust system at the selected field area formed in submarine conditions under several thousand meters of turbiditic sediments [*Teixell*, 1996]. We may therefore assume that erosion or syntectonic sedimentation did not have a significant effect on the structural variations at the scale of the individual thrusts as they crossed the stratigraphic units studied, whose thickness is of a few hundreds of meters. Modeling intended to investigate the effect of the following parameters: mechanical stratigraphy and sequence, competition between compositional-related behavior and stratigraphic position-related behavior (overburden), and strength of the décollement zone (i.e., high versus low friction).

[6] The loose sand used in the models is composed mainly of subangular quartz grains and has a coefficient of friction $\mu = 0.57$ ($\varphi = 30°$). Cohesion of loose sand typically ranges between 165–190 Pa [*Mulugeta*, 1988; *Liu et al.*, 1992]. The glass microbeads, provided by CBC Ytfinish Ab, are almost perfect spherical grains composed mainly of quartz glass (with minor components of Sodium and Calcium glass) with a grain size ranging between 100–105 microns and a bulk density of 1.5 g cm^{-3}. Their coefficient of friction is $\mu = 0.37$ ($\varphi = 20°$). Owing to its textural properties, loose sand compacts by loosing volume during model deformation, whereas glass microbeads, being made of subspherical particles, do not show this behavior. This means that while glass beads will accommodate layer-parallel shortening by bed thickening, sand will partly do it by volume reduction, although the amount of longitudinal shortening remain comparable. These are properties of the experimental materials not always directly applicable to natural deformation. Variations in décollement strength were investigated by using loose sand or glass microbeads at the décollement level. Models were 40 cm long in the undeformed stage, and were deformed in a pure shear box at the Hans Ramberg Tectonic Laboratory by a rigid backstop advancing at a constant speed of 0.3 mm/min.

2.1. Model Types

[7] We designed two types of models, a) thick, three-layered models with varied décollement strength (models 1 and 2), and b) thin, two-layer models with varied mechanical-stratigraphic sequence (models 3 and 4) (Figure 1). Marker points were placed on top of the models to track fault system kinematics (Figure 2).

[8] The three-layered models consisted of a weakening-upward stratigraphy with a basal layer of loose sand, an intermediate layer of sand/glass microbeads mixture, and an upper layer of glass microbeads, with marker seams of colored sand. Model 1 had a frictional décollement located at the interface between the sand and the metal base of the sandbox, whereas model 2 had a weak, low-friction décollement imposed within a basal cushion of glass beads. The two-layered models were all detached in a weak basal cushion of glass beads, and the deformed section consisted of one layer of sand and another of glass microbeads, both 6 mm thick, but with different stratigraphic sequence (model 3 had the sand at the base, whereas model 4 had the sand at the top) (Figure 1). A weak décollement was elected because, as discussed below, it enhances the mechanical expression of compositional contrasts. Shortening of the models by an advancing backstop on one end produced typical thrust-fold wedges (Figure 3).

2.2. Model Results

[9] In previous sandbox models with uniform material, the main variable that controlled the deformation style of

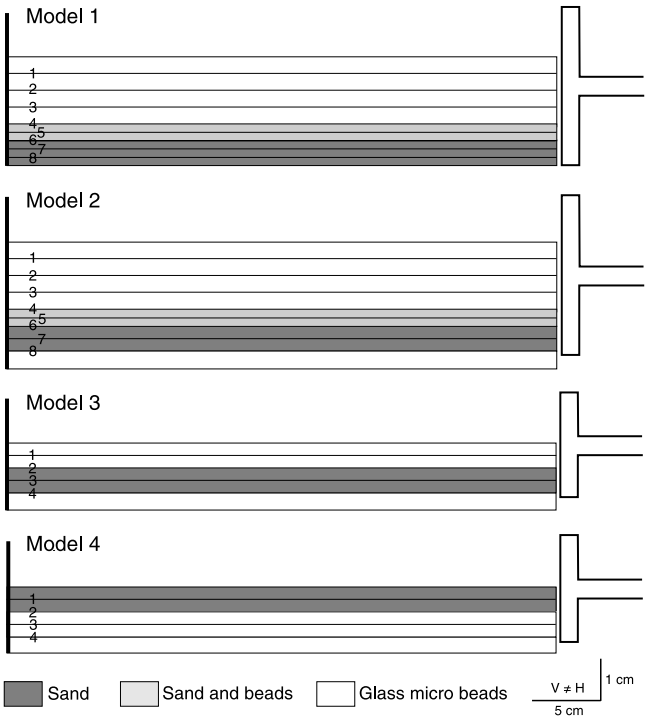

Figure 1. Types of models performed in this study, prior to backstop advance from the right. Numbers correspond to marker levels referred to in Figures 5 and 6.

each layer and the distribution of shortening modes was the overburden, i.e., the layer depth within the sand pile [e.g., *Mulugeta and Koyi*, 1987, 1992; *Marshak and Wilkerson*, 1992; *Koyi*, 1995]. Experiments reported in these works show a progressive increase in "ductility" with depth, related to increased compaction of sand aggregates and enhanced layer-parallel shortening.

[10] The experiments we performed combining granular materials of different mechanical properties altered this simple trend. The contrasting deformation styles can be readily perceived by visual inspection of the cross sections cut in the models (Figures 3 and 4) and was quantified by 1) recording the partition of shortening modes in each of the layers, 2) measuring fault displacement of different layers, and 3) tracing fault-related deformation zones. These features are described in detail below.

2.2.1. Shortening Partition

[11] The total, known bulk shortening in the models was factorized by means of bed length restoration (see description of the method by *Mulugeta and Koyi* [1987]) in components of thrust imbrication, folding, and distributed deformation. Weakening-upward models 1, 2 and 3 showed an inversion of the general trend of increased ductile deformation with depth. In these three models, the sand layers, despite their greater burial, accommodated 60 to 63% of the total shortening by thrust imbrication (Figures 5a–5c). Only the lowermost sand layer near the high-friction décollement of model 1 experienced less amount of imbrication shortening, due to drag at the adherent base of the wedge. In the three mentioned models, shallower glass bead layers were dominated by folding and distributed layer shortening, where the percentage of thrust contraction was only between 20 to 36% (Figures 5a–5c). The layers composed of sand/glass bead mixture showed an intermediate behavior, closer to that of sand (51–53% shortening by imbrication).

[12] This trend in shortening partitioning was reversed in model 4, where a deep-seated glass bead layer acquired only 27% of the total shortening by imbrication, and the overlying sand accommodated some 45% by this mechanism (Figure 5d). In this model, glass microbead layers appear intensely folded, and the sand layer is disharmonically imbricated on top of it (Figure 5d). However, in this model the proportion of shortening by thrust displacement in the sand layer (about 44%) is lower than in model 3 where the sand layer was at the base of the model. Even though sand was closer to the surface, in model 4 there was a significant percentage of shortening accommodated by folding, guided by the weak cushion of glass microbeads which formed the lower half of the wedge, in a way reminding buckle folding of natural competent units above more ductile substrata. A similar observation has been reported by *Koyi et al.* [2003], where sand layers shortened above a ductile layer underwent smaller amounts of layer-parallel shortening compared to sand layers shortened above a frictional décollement.

[13] Distributed layer-parallel shortening was variable but accounted for ca. 18–32% of the total bulk contraction in most layers (except those immediately overlying the décollement where it could be higher). Fold shortening was even more variable, but it showed a tendency to balance variations in imbrication shortening (Figure 5), suggesting a close association between the two mechanisms. *Koyi* [1995] demonstrated that layer-parallel shortening in sand wedges occurred rather independently and early in the deformation history, prior to the nucleation of folds and thrusts. With respect to the partition between folding and layer-parallel shortening in our models, sand-bearing layers experienced comparable amounts of the two or slightly greater amount of distributed shortening, whereas folding clearly dominated

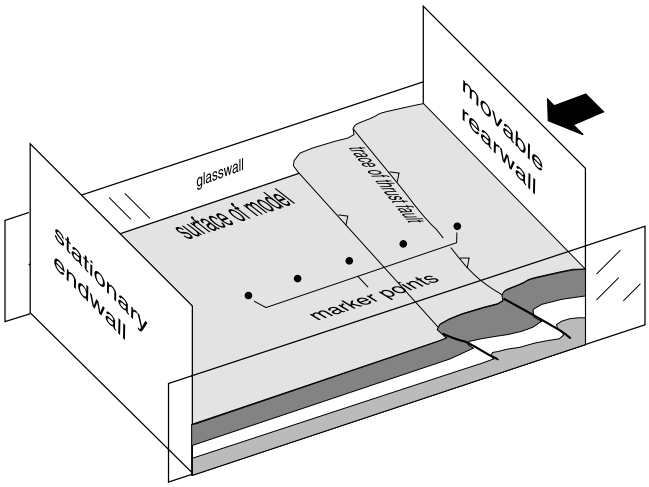

Figure 2. Block diagram of a deformed model with marker points on top to track fault kinematics.

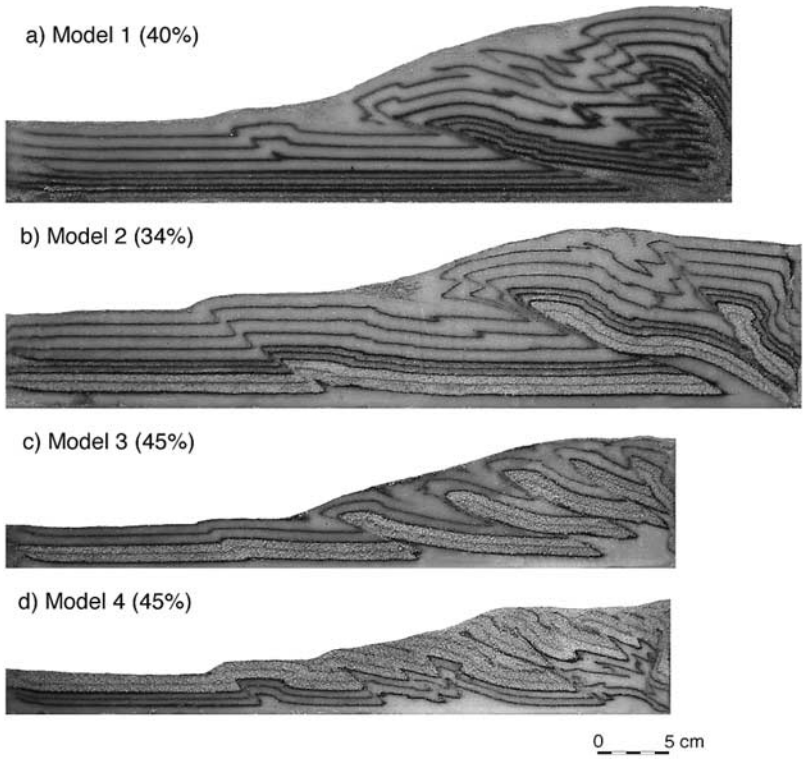

Figure 3. Photographs of selected sections of the four deformed models. (a) Model 1, with three mechanical layers and a frictional base. (b) Model 2, with the same stratigraphy as model 1, but with lower friction at the base. (c and d) Two-layer models 3 and 4, with low-friction décollements but different stratigraphic order. See Figure 4 for layer compositions.

in layers composed exclusively of glass microbeads. This can be attributed to the packing properties of the modeling materials (some layer shortening in loose sand occurs by compaction, and glass microbeads are little compactable).

[14] By comparison, a compositionally homogeneous sand wedge analyzed by *Mulugeta and Koyi* [1987] showed a continuous increase in layer shortening with depth (from 40% at the top to 90% at the base), and a decrease in imbrication (from 45% to less than 5% at the base), abruptly falling at midstratigraphic levels. Fold shortening showed only a gentle decrease downsection. This is a typical behavior of frictional modeling materials. *Liu and Dixon* [1991] found the opposite distribution using non-Newtonian viscous materials, which are appropriate analogue materials of upper crustal deformation only in special cases.

[15] The presented results show that the prime controlling factor in the deformation style in models with layers of different composition were the intrinsic mechanical properties of each of the layers, dominating over the effect of overburden. On the other hand, the comparison of models 1 and 2, which were shortened above a high-friction and low-friction décollement respectively, suggests that the strength of the basal décollement affects the distribution of shortening components across the mechanical stratigraphy. In both models, the layers of sand and sand/beads mixture experienced almost the same percentage of shortening by thrust displacement (62 and 60% for sand, 52 and 51% for mixture), whereas pure glass bead layers behaved differently: 35% in average of the total shortening was accommodated by imbrication in the high-friction décollement model 1, compared to an average of only 23% in the low-friction décollement model (2) (Figures 5a and 5b). These data, together with a simple visual inspection of the two models, suggest that the strength of the décollement level influenced the differences in behavior of layers of different composition: low basal friction seemed to enhance mechanical contrasts and disharmony, whereas high basal friction had the opposite effect. High friction induced more coupling between layers and enhanced ductile deformation.

2.2.2. Thrust Geometry

[16] In the model wedges, thrust fault zones could be narrow or diffuse, and formed always homoclinal ramps that cut the entire succession (Figures 3 and 4). Ramp-flat geometries as those obtained by *Turrini et al.* [2001] in alternating sand and glass microbeads multilayers did not develop, as individual thrusts showed rather homogeneous dips. This allowed tracking variations in structural style along a single fault as it crossed layers of different material.

[17] Disharmony between layers of different nature was frequently observed. Sand layers were cut by narrow thrust zones, which when passing upsection to glass microbeads branched into several splays, or graded to tight folds with sheared forelimbs, or to box folds (Figures 3 and 4). This is coherent with shortening being accommodated by different

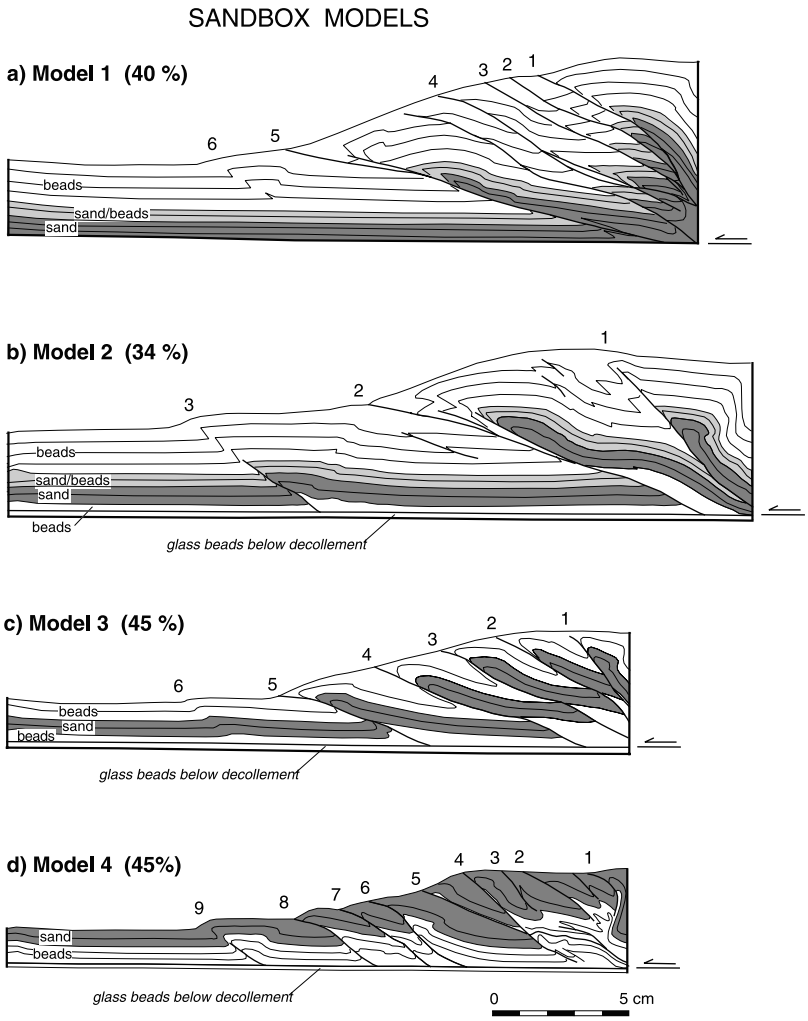

Figure 4. Sketches of the model sections of Figure 3. Numbers on top indicate the main thrust faults referred to in Figure 6. Numbers on the left refer to marker levels.

mechanisms in each mechanical-stratigraphic unit, as has been documented quantitatively above. Initial ramp dips, where not affected by back rotation, ranged usually from 15 to 20° in weakening-upward models (Figures 4a–4c), and were slightly greater in strengthening upward model 4 (Figure 4d). In models detached in a weak glass beads cushion, the lowermost part of the ramps had a steeper inclination (even when cutting sand, e.g., Figure 4c), due to penetrative shortening and rotation.

[18] Spacing of thrust faults was primarily controlled by the strength of the basal décollement, as illustrated by a comparison of Figures 4a and 4b. This result, which is related to the critical taper of the sand wedge, is coherent with previous works [e.g., *Mulugeta*, 1988], and will not be discussed further. Changing the mechanical-stratigraphic order had a smaller effect on thrust spacing (Figures 4c and 4d). Somewhat higher spacing was observed in the weakening-upward model 3, where the ratio between the line-restored length of each imbricate to the stratigraphic thickness of the model averaged 4.1. In the strengthening-upward model 4 an average ratio of 2.7 was observed. In homogeneous sand models, *Mulugeta* [1988] obtained an average ratio of 4.8 (thrust imbricates closer to the backstop were not considered).

[19] In model 1, the frontalmost structure was a detachment fold above a minor décollement between glass beads and underlying sand (Figure 4a). However, this detachment did not segment the nearest ramp at the rear, despite the structures formed in a piggyback sequence. Inspection of ramp-flat models by *Turrini et al.* [2001, Figures 2 and 5] reveals the same effect: ramps are not segmented by flats emanating from the middle of them, despite their propagation in piggyback fashion. This indicates local balance of shortening, e.g., the lower part of the section was shortening homogeneously and the upper part, above the flat, was contracting by folding and/or imbrication. Another interesting effect, shown by models 1 and 2, is the development of hanging wall flats not matched by corresponding flats in the footwall. This is due to enhanced ductile deformation at the lowermost levels (see *Koyi and Teixell* [1999] for a full discussion). These two observations, although largely determined by the physical properties of the modeling materi-

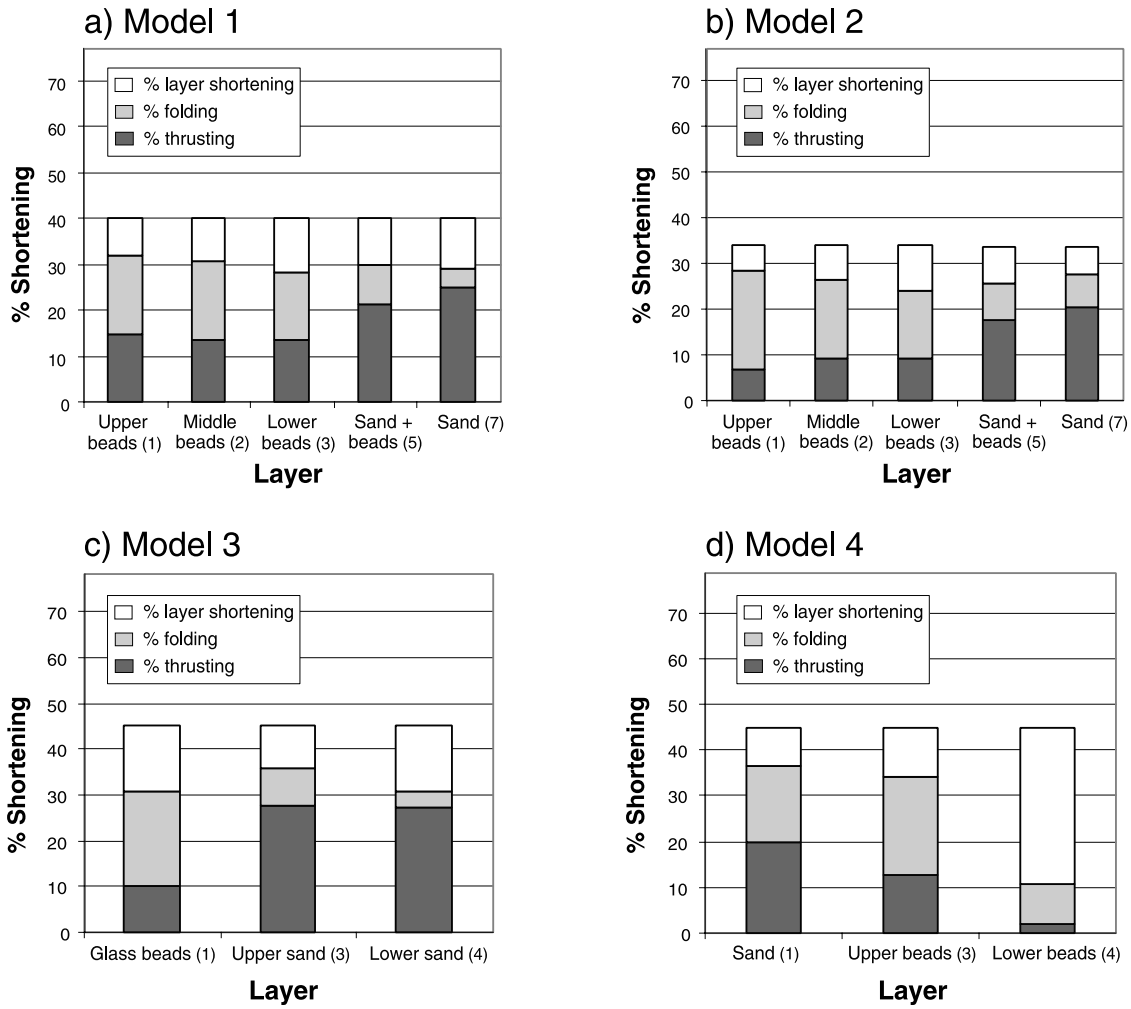

Figure 5. Diagrams showing the partition of shortening into different mechanisms for layers of diverse composition in (a) model 1, (b) model 2, (c) model 3, and (d) model 4. See Figures 1 and 4 for layer numbers.

als, warn about the indiscriminate use of the classic geometric rules (i.e., template constraints) when constructing cross sections of thrust belts.

2.2.3. Displacement Variation

[20] The contrasting behavior of the different mechanical stratigraphic units is also expressed by the displacement variation along individual thrust faults. The recorded values for the study models are presented in Figure 6. In general these results are consistent with the distribution of shortening mechanisms discussed above. Again, the fault displacement of a particular layer is governed principally by its composition. As expected, slip was greater in sand layers irrespective of their position. Displacement decreased nonlinearly upsection in weakening-upward models (1, 2 and 3), and increased in the strengthening-upward model 4 (Figures 6a–6d). Displacement reduction when passing from sand to glass microbeads is especially large in model 3 (Figures 4c and 6c).

[21] *Ellis and Dunlap* [1988], attributed displacement variations in natural faults to punctual fault nucleation and subsequent propagation. Thrust zones in sandbox models nucleate as rather harmonic kink bands (e.g., structure 6 in Figure 4c), which thin to discrete faults by internal rotation [*Mulugeta and Koyi*, 1992; *Storti et al.*, 1997]. This behavior, common in granular materials, is a valid analogue to understand relationships between fault propagation, slip and folding. In our models, the bands rotated faster into a narrow thrusts in sand than in glass bead layers, where they evolved to a wider and amplified fold. This is analogous to fault propagation folding in nature, but it is interesting to note that in the models, displacement variation was greater for thrusts with greater finite translation (Figures 6c and 6d). Part of the displacement variation may have been achieved after the failure had already propagated, resulting from changes in the ratio of the resistance to slip to the resistance to internal deformation or folding.

2.2.4. Folding and Thrust Zone Deformation

[22] In all models, narrow thrust faults in sand passed to wider deformation zones and folds in glass microbeads

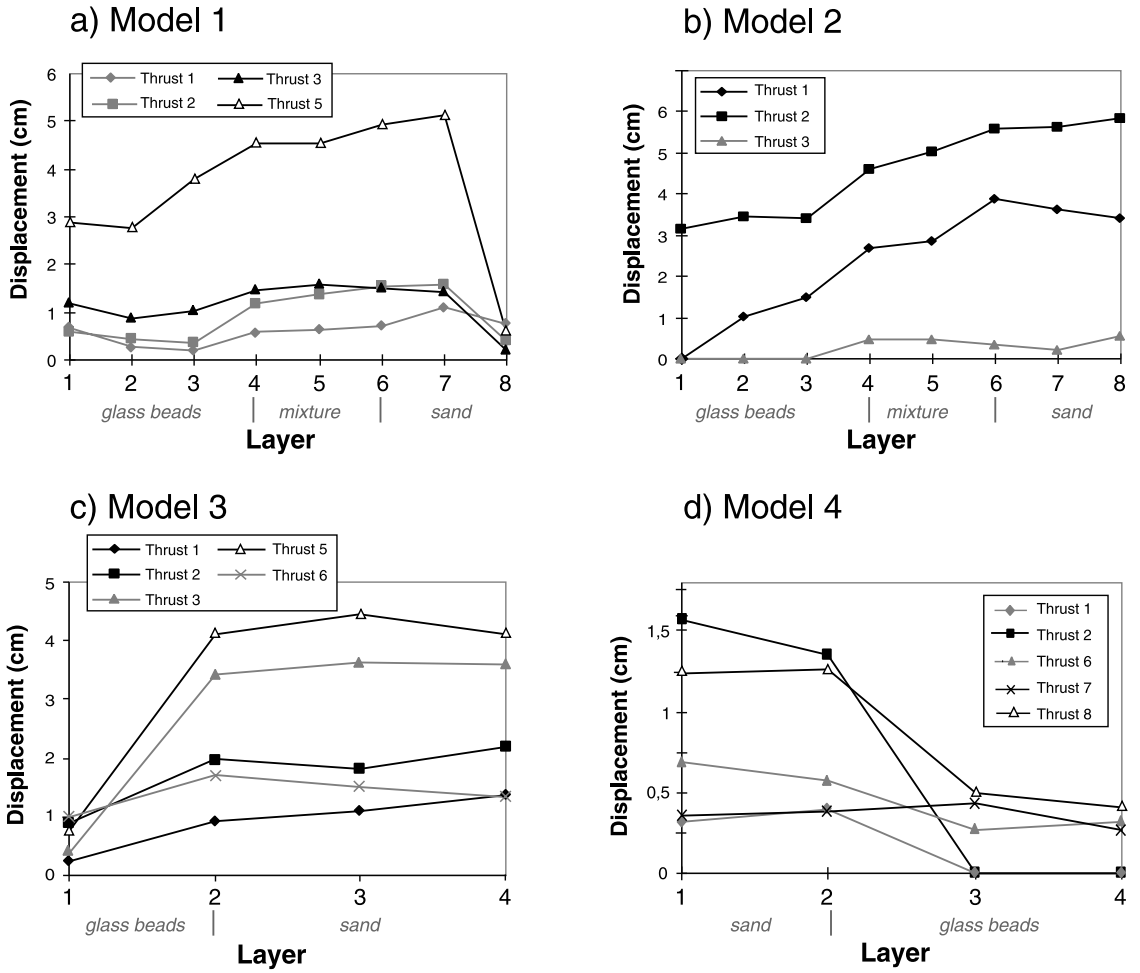

Figure 6. Diagrams of displacement variation for selected thrust faults in the deformed models: (a) model 1, (b) model 2, (c) model 3, (d) model 4. See Figure 4 for thrust and layer numbers (for each diagram, layer numbers increase with depth).

(Figures 3 and 7). This happened upsection or downsection, according to the stratigraphic order. When a thrust brings in contact layers of both types of materials (i.e., loose sand and glass microbeads) at the same level, the deformation zone is asymmetric with respect to the fault: it is wider in glass microbeads. Folds were asymmetric hanging wall anticlines and footwall synclines, with sheared forelimbs. As discussed above, folding accommodated displacement reduction along single faults. These features are taken as indicative of fault propagation folding in natural thrust tectonics; in the study experiments they could have been enhanced by variations in slip/folding ratio between different mechanical-stratigraphic units once the failure had propagated through the entire section.

[23] Thrust deformation zones passing from sand to glass bead units had roughly triangular or funnel-shaped geometries in profile, recalling the trishear folds described by *Erslev* [1991] and *Hardy and Ford* [1997]. Existing numerical models of trishear fault propagation folds are determined by the imposed direction of fault propagation, and by predefined propagation/slip ratios in lithologically uniform successions [*Hardy and Ford*, 1997]. *Alonso and Teixell* [1992] described natural examples of triangular-shaped, heterogeneous shear zones in relation to faults where the propagation/slip ratio varied along single faults as they cut through rocks of different composition. A comparable effect was replicated in the models, as expressed by variation of the width of the deformation zones (Figure 7), be it by changes in slip to propagation ratio or by changes in resistance to slip in already propagated faults.

2.2.5. Wedge Taper

[24] Sandbox experiments have been extensively used to model wedge taper attributes [*Davis et al.*, 1983; *Mulugeta*, 1988; *Mulugeta and Koyi*, 1992; *Liu et al.*, 1992; *Koyi*, 1995; *Gutscher et al.*, 1998]. *Liu et al.* [1992] investigated the development of wedges under different values of frictional coupling along the décollement surface, by detaching sand from diverse types of substrata. As expected, friction increased critical taper angles (1.5° for a basal friction $\mu_b = 0.37$, and up to 16°–20° for high-friction substrata), although model sand wedges seldom attain tapers predicted by Coulomb wedge theory [*Liu et al.*, 1992; *Koyi*, 1995].

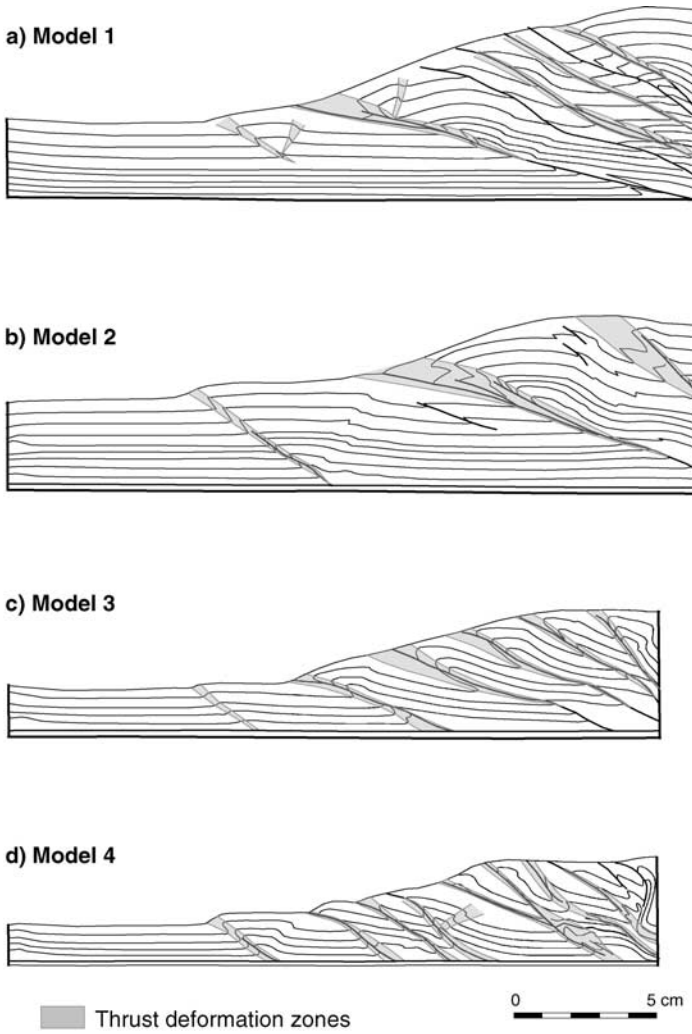

Figure 7. Simplified sketch of the deformed models indicating the thrust deformation or damage zones: (a) model 1, (b) model 2, (c) model 3, (d) model 4.

[25] The evolution of wedges made up of layers of different mechanical properties (and in different stratigraphic order) is poorly known, as critical wedge theory considers constant material properties within the wedge. Model 1, detached on a frictional substratum, developed a taper comparable to those of previous works [*Liu et al.*, 1992; *Koyi*, 1995], but the models detached within glass microbeads (μ_b = 0.37) attained much higher tapers than those with comparable basal friction of *Liu et al.* [1992] (up to 10°–15°).

[26] In our experiments, it appears that the strength of the stiff sand layer within the succession guides the taper of the whole imbricate system. In model 3, a fairly regular ramp spacing and fault displacement is controlled by the rheology and thickness of the stronger sand layer, whose fold envelope (as defined by the leading edges of the imbricate slices) matches the surface slope of the wedge, which is close to 14° (Figure 4c). Thicker wedges in models 1 and 2 showed the same feature. This has implications for natural examples where posttectonic erosion has obscured the shape of the original, complete wedge. Interestingly, model 4, which had the same décollement character and the same bulk mean composition as model 3 but with reverse stratigraphic order, attained a gentler taper angle (11°). Still, this angle is quite high for the weak décollement, but it is worth to note that the sand layer, now in the upper stratigraphic position, is again guiding the wedge: the fold envelope defined by the leading edge of the deformed glass bead layer is only inclined 6°, and the overlying sand layer piled up in a way that increased surface slope (Figure 4d).

3. Field Example: The Aragüés Imbricate System

[27] The Aragüés thrust system of the Spanish Pyrenees is an excellent natural example to study variations in deformation style guided by the mechanical stratigraphy. This imbricate thrust system involves upper Cretaceous to

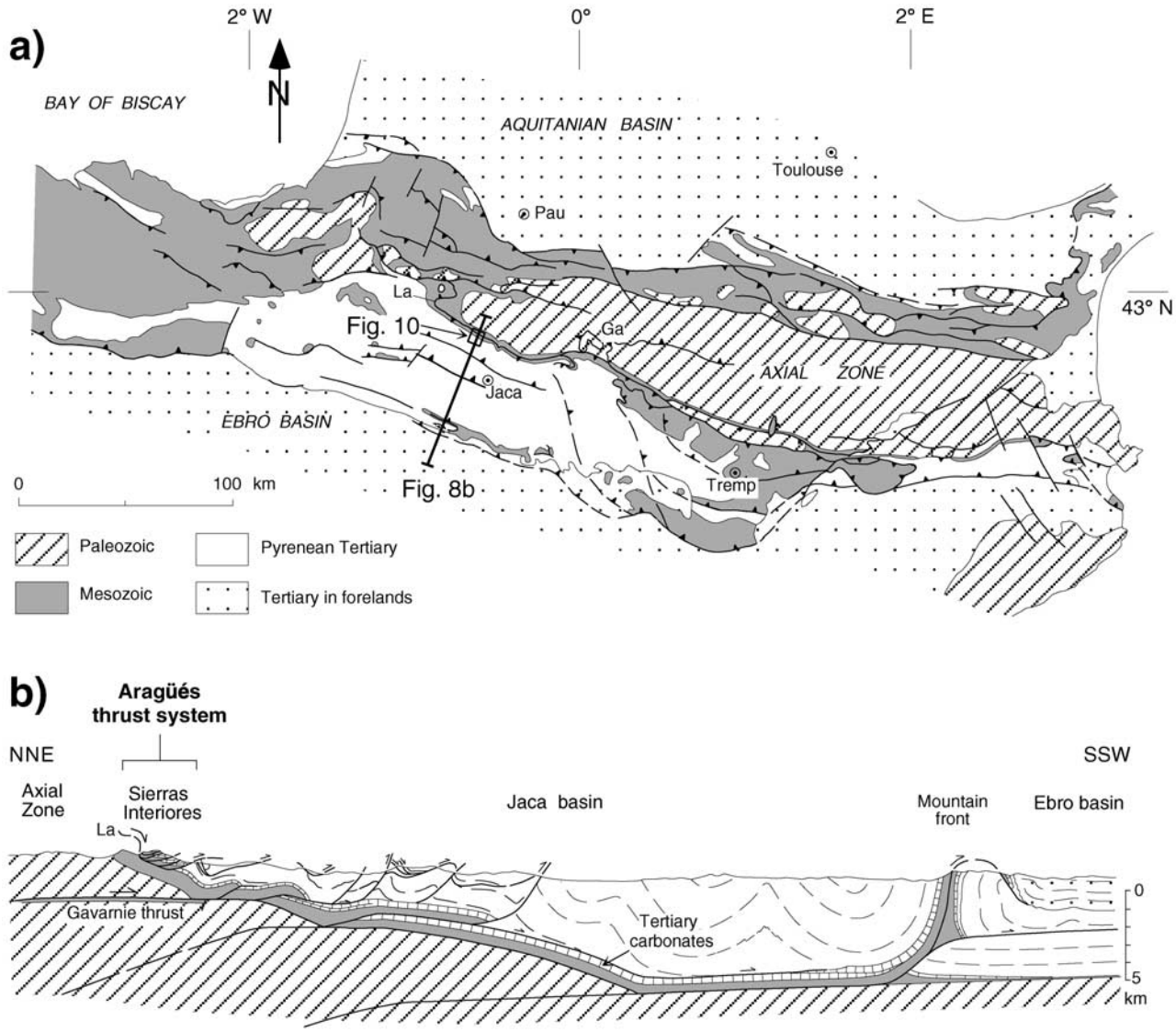

Figure 8. (a) General geologic map and (b) cross section showing the setting of the Aragüés thrust system in the Pyrenean orogen. La, Larra thrust; Ga, Gavarnie thrust.

lower Tertiary sedimentary rocks, and developed during the Eocene under a thick cover (some 4 km) of turbiditic sediments. The imbricates were later uplifted and exposed by an underlying basement-involved thrust, which raised the system in the southern limb of the Axial Zone basement massif of the Pyrenees (Figure 8). Aspects of regional structure are described by *Van Elsberg* [1968], *Labaume et al.* [1985], and *Teixell* [1990, 1996].

[28] A profile of the thrust system is spectacularly exposed in a 1300 m deep canyon at the head of the Osia river valley, north of the village of Aragüés del Puerto. The area shows a distinctive stratigraphy that consists of contrasting lithologies. Many key structural relationships can be directly observed in outcrop, making the area very suitable for the analysis intended (Figure 9). The field analysis included structural mapping on aerial photographs enlarged to approximately 1:4500 scale, combined with detailed outcrop study. Figure 10 shows a simplified map of the area, and two cross sections are presented in Figure 11.

3.1. Lithostratigraphy

[29] The Aragüés thrust system was developed in layered sedimentary rocks which can be divided into several stratigraphic units, each of them with a characteristic behavior during tectonic deformation (Figure 12). The lowermost unit involved in the imbricate system is the Marboré sandstone formation, (Maastrichtian [*Souquet*, 1967]), which is tectonically detached from an underlying assemblage of calcareous shale (marl) and shaly limestone (Zuriza formation, Campanian-lower Maastrichtian).

[30] The Marboré sandstone is composed of decimetric to metric-scale layers of grey, brown-weathered quartz carbonate sandstone. As seen in thin sections, it ranges

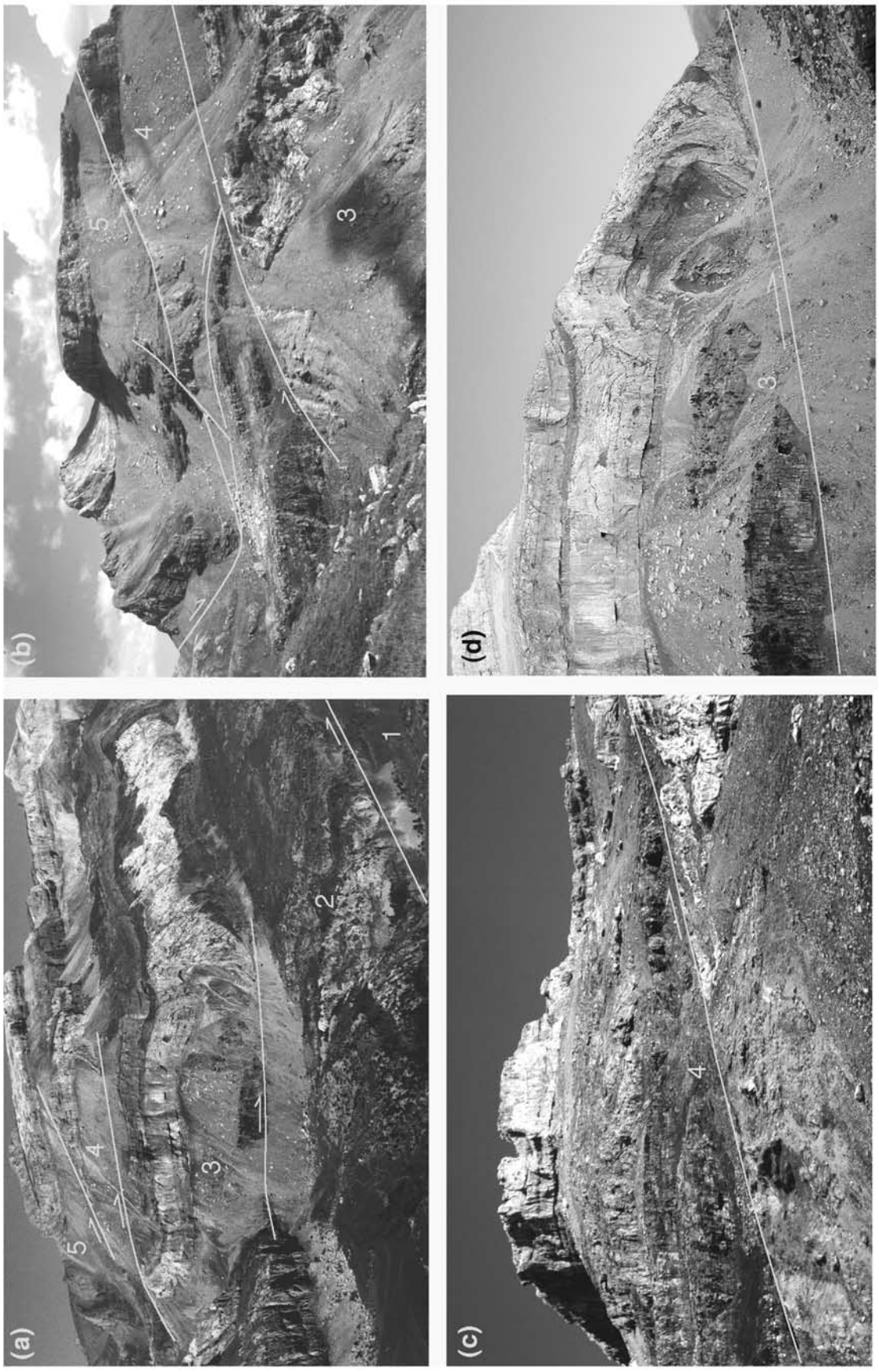
(a)
(b)
(c)
(d)
1
2
3
4
5

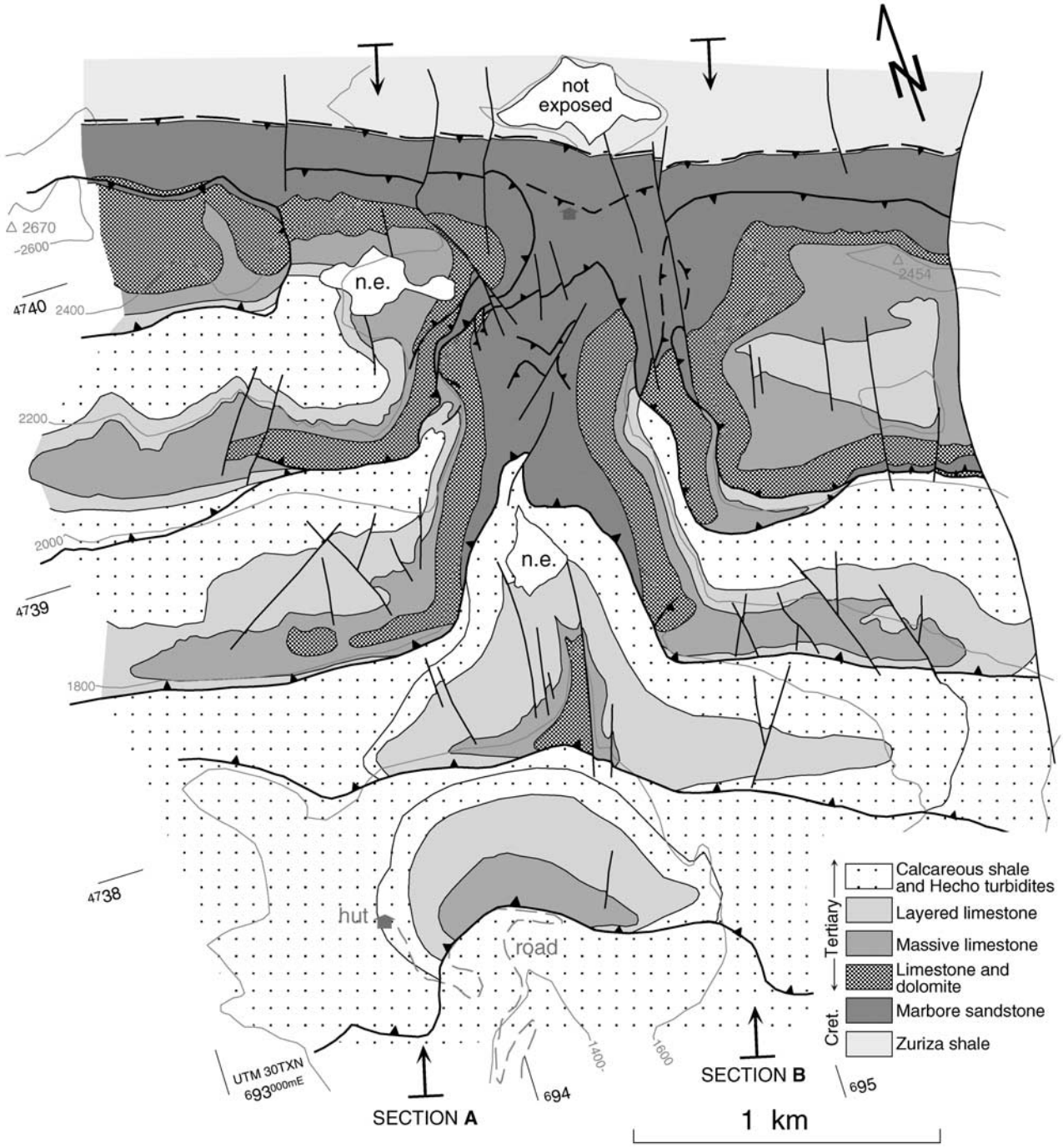

Figure 10. Geological map of the Aragüés thrust system in the Osia valley.

Figure 9. (opposite) Field photographs of the Aragüés thrust system. (a) Panoramic view of the Osia valley and the entire thrust system from the southwest. (b) Photograph looking east of the northern part of the system. The Marboré sandstone appears brown-weathered in the center and left, whereas the white cliffs correspond to the Tertiary carbonates. The slope is ~500 m high. Compare with the cross section of Figure 11b. (c) Ramp of thrust 4 in the eastern side of the valley. The Marboré sandstone is in the nearest hanging wall (brown), and the Paleocene dolomite (grey) and massive limestone (white) are in the footwall. The image is ~250 m wide. (d) Frontal box fold at the leading edge of thrust unit 3, very similar to those obtained in analogue models. The field of view is ~500 m wide, and north is to the left. The Marboré sandstone (lower left) shows a gentle cutoff angle; the poorly exposed unit is the massive dolomite, and the overlying limestone units show a overturned box fold with marked forelimb thinning. See color version of this figure at back of this issue.

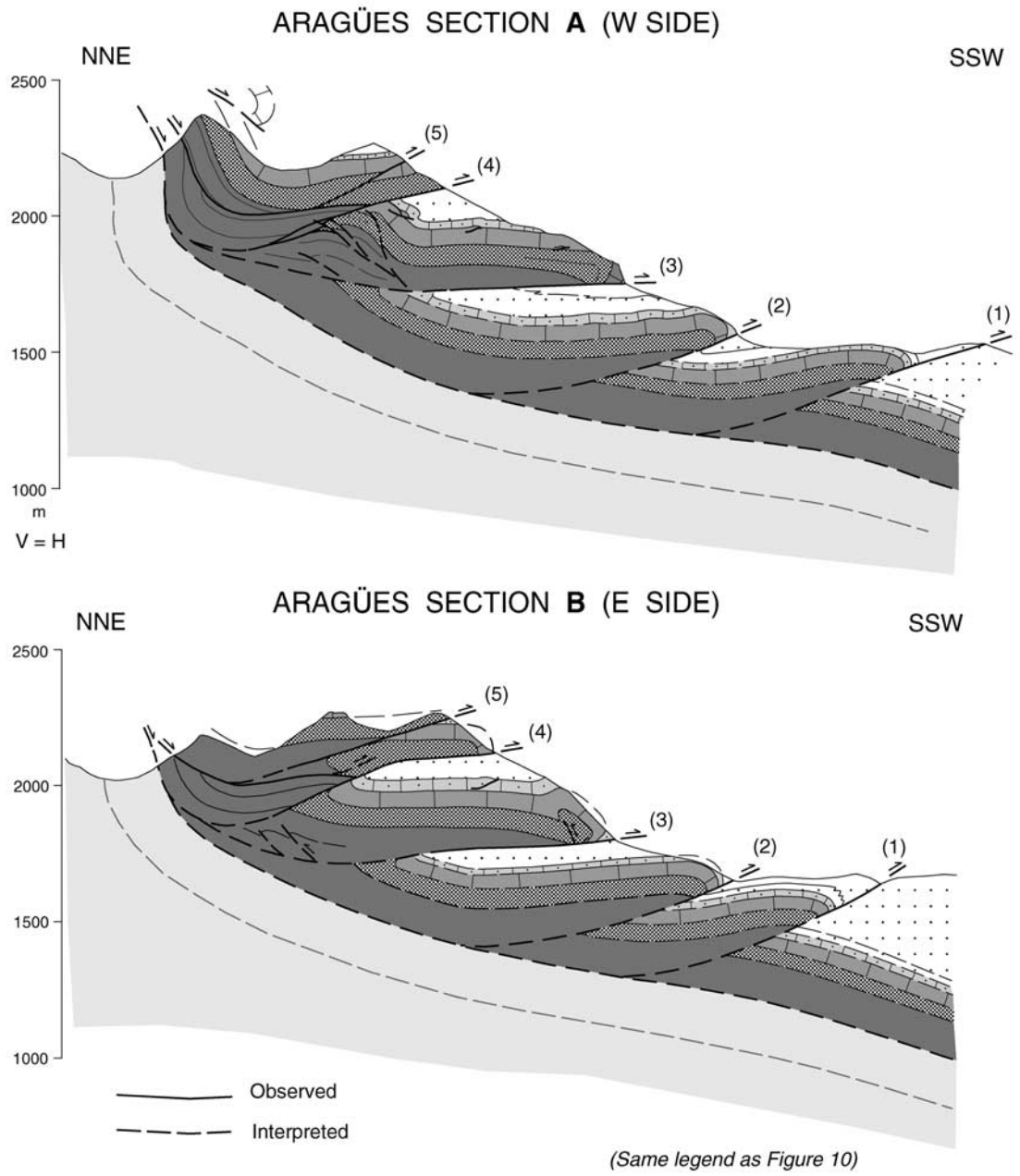

Figure 11. Structural cross sections through the Aragüés thrust system on both sides of the Osia river: (a) west side and (b) east side. See Figure 10 for location and legend of stratigraphic units.

from grain-supported quartzarenite with sparse carbonate cement to matrix-supported greywacke with quartz and calcite grains enclosed in a carbonate matrix. Pure pelitic layers are usually absent, except at the base of the formation, which is transitional to the underlying Zuriza shale, and at some very thin argilaceous interbeds. The Marboré sandstone is well bedded, in decimetric to metric-scale layers, commonly separated by planar parting surfaces. The total thickness of the formation in the Aragüés area is difficult to estimate as it is truncated by thrust faults, but cross section construction constraints and information from adjoining areas allows an estimate close to 150 m.

[31] The Marboré sandstone is stratigraphically overlain by a group of white/light grey dolomites and limestones of Tertiary (Paleocene-lower Eocene) age, which can be subdivided into several subunits (Figure 12). The total thickness of this carbonate group varies from 130 to 175 m. The basal member consists of crudely bedded, grey sacaroidal dolomite made up of idiomorphic dolomite crystals which occasionally preserve ghosts of fossil fragments (mainly single-crystal grains with syntaxial cement). This unit is

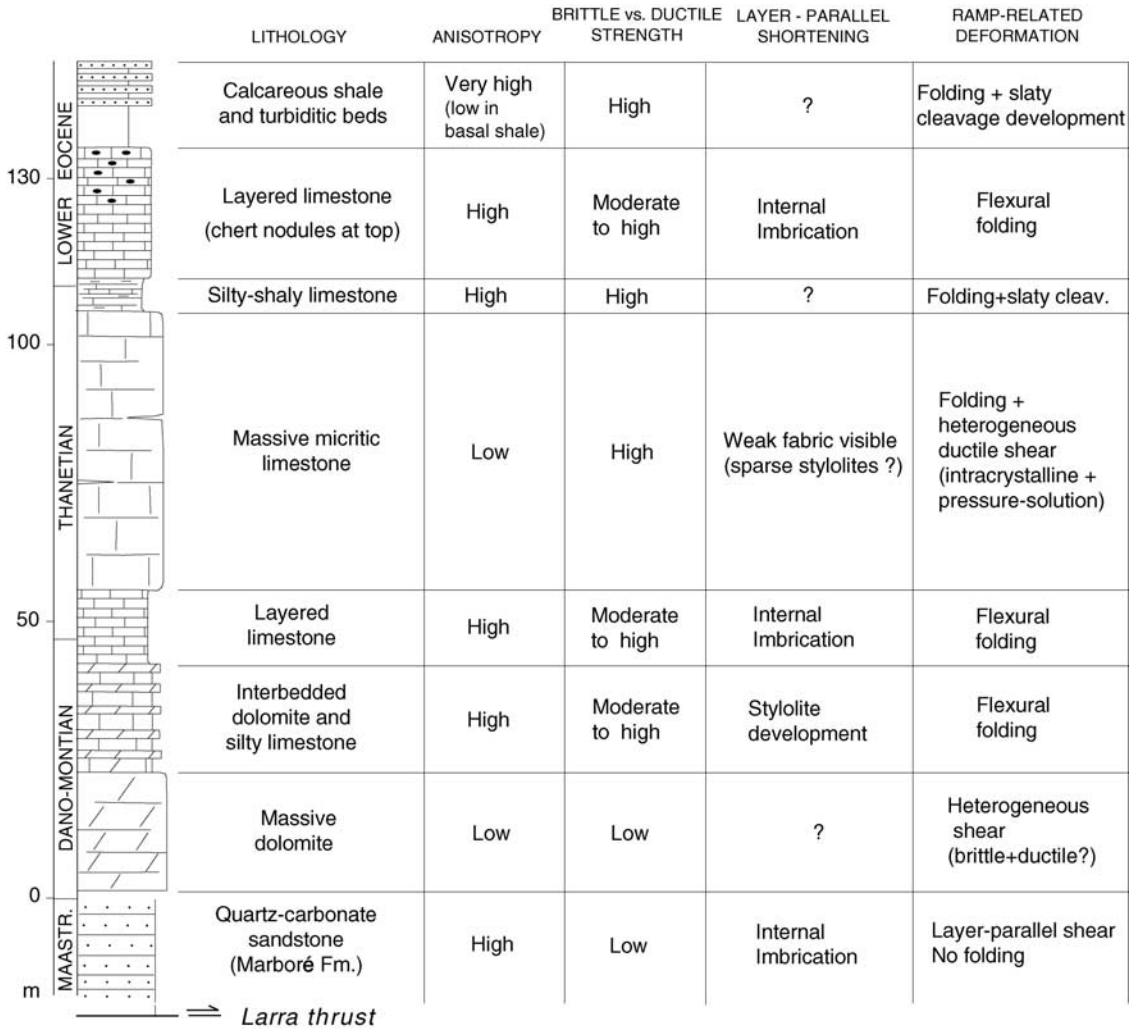

Figure 12. Mechanical-stratigraphic log of sedimentary units involved in the Aragüés thrust system. "Brittle versus ductile strength" refers to the brittle strength relative to the inferred ductile strength.

overlain by alternating dolomite and silty bioclastic limestone, and then by well-bedded micritic and bioclastic limestone (mudstone-wackestone) (Figure 12) These two units are arranged in metric-scale layers, separated by planar to undulose parting interfaces, occasionally stylolitic. The next unit is a massive packet of micritic limestone which often forms a characteristic white cliff. The limestone ranges from mudstone-wackestone to algal-coral boundstone, well-cemented and competent. Bedding in this unit is poorly defined. It is followed abruptly by a thin unit of well-bedded grey to brown sandy limestone, with pelitic, centimetric interlayers, and then by purer well-bedded limestone (mudstone-wackestone in metric-scale layers) with abundant bioclasts and chert noduli, which belong to the lower Eocene (Figure 12).

[32] The carbonate group described above is overlain by less competent rocks in which thrust faults are usually more difficult to follow. These rocks begin with cleaved grey to yellowish marls (10 to 60 m) with sparse carbonate breccia layers, followed by siliciclastic turbiditic beds (Hecho group [*Mutti*, 1984]), that form a typical foreland turbiditic wedge that in the whole of the Jaca basin can reach a thickness of over 4000 m (Figure 8b).

3.2. Structural Geometry and Kinematics

[33] The Aragüés thrust system involves the Marboré sandstone, the Tertiary carbonates and the lower part of the marly/turbiditic succession (Figure 10). Two detailed cross sections, of each side of the Osia canyon, have been constructed (Figure 11). Thrusts form a 3 km across imbricate stack of 5 slices that is tilted and folded into an asymmetric syncline (Bernera syncline). The Bernera syncline postdated the formation of the imbricate system itself, and is attributed to folding in the hanging wall ramp of the deeper-level Gavarnie thrust (Figure 8b). During this second-stage of deformation, the leading edges of the imbricate thrust sheets were not significantly distorted, whereas the trailing edges were rotated to near-vertical position in the forelimb of the Bernera syncline (Figures 11 and 13).

Figure 13. Footwall ramp within the Marboré sandstone in the rear of thrust 5. North is to the left. Note that the thrust dips in the direction of tectonic transport (to the south), an effect caused by postthrusting deformation expressed as the Bernera syncline. The slope is ~200 m high.

[34] Individual ramps converge in a bedding-parallel floor thrust located at the base of the Marboré sandstone. This floor thrust, called the Larra thrust [*Teixell*, 1990] fits strictly the décollement definition as it causes no stratigraphic repetition. The underlying Zuriza shale appear only affected by folding and associated cleavage related to the later Gavarnie deformation. Within each of the imbricate thrust sheets, hanging wall ramps and cutoffs are very well exposed, whereas footwall ramps, especially in the lower sheets, are less exposed. Well-developed fault-related folding is observed in exposed ramp regions (Figure 11), consisting essentially of asymmetric, overturned hanging wall anticlines.

[35] The general strike of the thrust system is WNW-ESE, whereas the direction of climb of thrust faults across the stratigraphy and the vergence of folding are both to the SSW. Cutoff lines based on present outcrop consistently trend N112-N114 for thrusts 2 to 4 (Figure 14), and N100 for thrust 1 (Table 2). Thrust 5 shows an oblique cutoff trend, due to lateral displacement reduction from east to west. Slip lineations oriented N017 have been observed at the base of thrust 3. Cross sections have been drawn with N017 orientation, approximately parallel to the assumed regional transport direction. In addition, branch line orientation independently deduced from cross section construction have consistent trends: N100 for the branch line between thrust 1 and the floor thrust, and N111-N112 for thrusts 2 and 3 (Figure 14). Southward displacement of the individual imbricate thrusts is of the scale of hundreds of m (Table 2).

3.2.1. Thrust Attitude and Spacing

[36] Initial ramps dips are difficult to evaluate, due to postthrust deformation and incomplete footwall exposure, but section restoration suggests it was broadly about 10°–20° (Figure 15). As a general rule, the Marboré sandstone is cut by the imbricate thrusts in gentle cutoff angles (10°–14°) (Figure 9c), whereas Tertiary carbonates are usually overturned and cut by the thrust ramps at angles between 120° and 160° (counted clockwise; e.g., Figure 9d).

[37] The restored length of each of the thrust sheets (Table 2), taking the top of the Marboré sandstone as reference horizon, on which we have a good outcrop control, is about 900 m in average. Dividing the length of each imbricates by the total thickness of sandstone and carbonate formations yield ratios roughly between 2 and 4 (Table 2). These ratios are the same order of magnitude as those in the analogue models, and indicate that it was these relatively competent formations which controlled thrust spacing, whereas the much weaker, and thicker, turbiditic group on top of the succession had minor effect.

3.2.2. Fault-Related Folding

[38] While the Marboré sandstone dips rather homoclinally and abuts against the thrusts at gentle ramp angles, the overlying Tertiary carbonates show fault-related folds (Figure 9), a feature described in detail by *Alonso and Teixell* [1992]. This is the first striking contrast in terms of mechanical behavior in relation to the stratigraphy. *Alonso and Teixell* [1992] related this contrast to a lithologically controlled variation in slip/propagation ratio, being higher in the sandstone and lower in the carbonates, which developed fault propagation folds. The folds are very

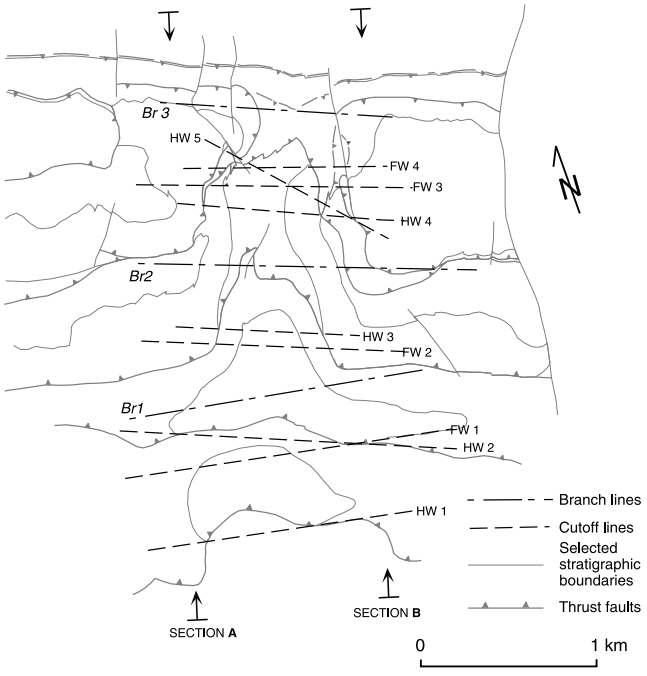

Figure 14. Branch and cutoff line map of the Aragüés thrust system.

Table 2. Summary of Field Data of the Aragüés Thrust System (Based Mainly on Section B)[a]

Thrust	Cutoff Trend		HW Cutoff Angle,[b] deg		Fold Axial Angle,[c] deg		Thrust Displacement		Restored Length,[d] min	Length/ Thickness Ratio[e]
	HW	FW	Sandstone	Limestone	γBL	γFL	Top of Sandstone	Base of Limestone		
5	N133	N128	14–16				218		970	3,2
4	N114	N109	14–18	90	47	53	723	557	543	1,8
3	N112	N112	10–13	160	20	40–50	790	684	1048	3,5
2	N113	N112		117	38	55	437	333	1276	4,2
1	N101	N100					283	253	805	2,7

[a]All longitudinal data in m. "Limestone" refers to the massive paleocene limestone formation.
[b]Hanging wall cutoff angle counted clockwise from the thrust to bedding. Angles greater than 90° indicate overturned bedding.
[c]Values referring to the paleocene massive limestone formation. γBL, backlimb axial semiangle; γFL, forelimb axial semiangle.
[d]Values based on the top of the Marboré sandstone formation.
[e]Values based on the restored length of the top of the Marboré sandstone and the cumulative thickness of Marboré sandstone and Tertiary carbonates.

asymmetric. Their backlimbs are long and straight, with deformation accommodated mainly by layer-parallel (flexural) shear, as indicated by constant bed thickness and occasional bedding plane striations or oblique slaty cleavage in argillaceous interbeds. On the other hand, the forelimbs are curvilinear in profile, displaying progressive thinning of beds toward the fault surface (Figure 9d). *Alonso and Teixell* [1992] concluded that this geometry was the result of a complex and heterogeneous strain superimposed to flexural shear during fault-related folding, which was assimilated to a triangular-shaped, shear zone with diverging walls and extrusion. The shape of such deformation zone resembles that of the trishear fault propagation model of *Erslev* [1991], and their localization indicate a heterogeneous strain that is restricted to regions or lithologies where motion was inhibited (tip zones or ramps).

3.2.3. Displacement Variation

[39] Displacement along individual thrusts was measured taking as reference the tops of the sandstone, dolomite and limestone formations (Figure 16). Similar to the analogue models, thrust displacement of each layer varied in a consistent way according to its composition. Displacement was greater in the Marboré sandstone, and decreased upsection as the carbonates were folded. This could be attributed to stratigraphically controlled fault propagation folding, but in fact this mechanism is inseparable from differential slip/folding resistance ratio in each lithology after the fault had fully propagated. The superimposed

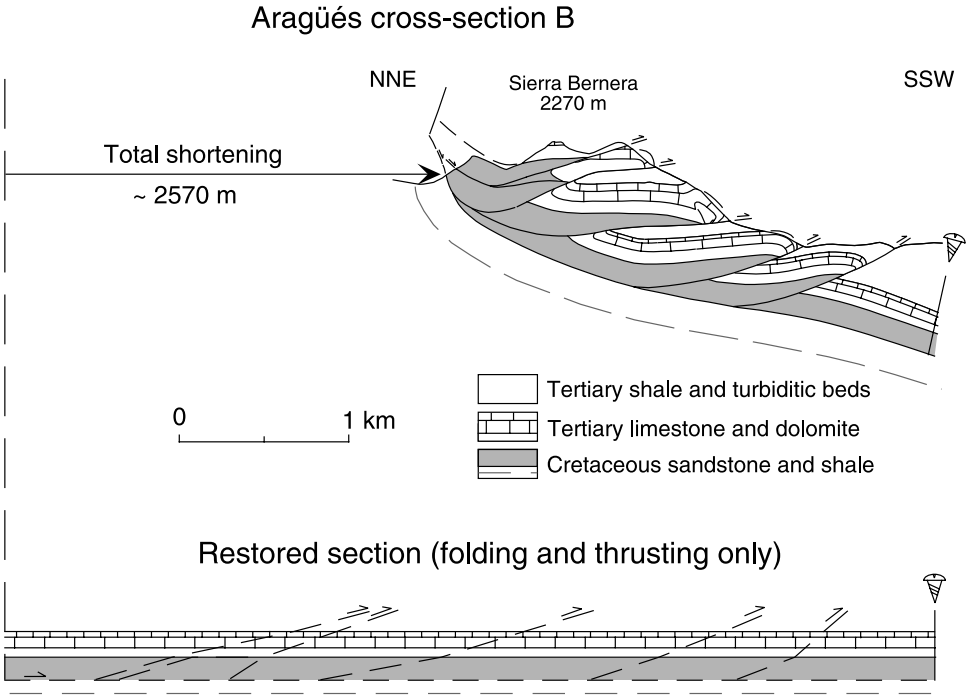

Figure 15. Comparison of present and restored sections of the Aragüés thrust system in the eastern side of the Osia valley.

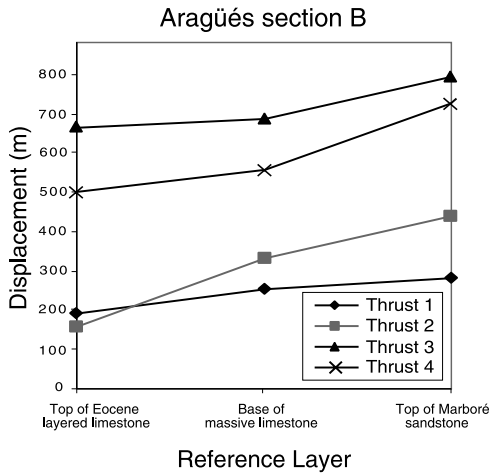

Figure 16. Diagram showing the pattern of displacement variation for selected thrust faults and reference layers of the eastern Aragüés section. Thrust numeration corresponds to that of Figure 11.

heterogeneous strain in fold forelimbs resulted in further reduction of cutoff lengths [*Alonso and Teixell*, 1992].

3.2.4. Shortening Partition

[40] The partition between folding and imbrication for each horizon is in accordance with the patterns of folding and displacement reduction (Figure 17). It is noteworthy that carbonates are more preferentially folded than the Marboré sandstone, which is layered and mechanically more anisotropic. The sandstone had probably lower relative ductility and brittle strength, offering less resistance to fault propagation or slip than the limestone.

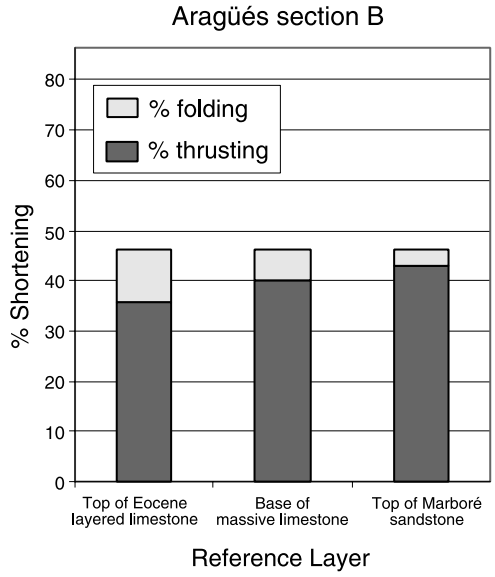

Figure 17. Diagram indicating the partition of shortening in thrusting and folding in layers of different composition at Aragüés. Layer-parallel shortening could not be quantified in a systematic way and was not considered in this analysis.

[41] The Aragüés imbricates experienced early layer-parallel shortening, as indicated by minor structures of different types, characteristic in each lithological unit (Figure 12). The Marboré sandstone and the layered limestone units experienced internal contraction by small-scale imbrication, which occurred early in the deformation history as it appears either tilted in large-scale fold forelimbs or truncated by the main thrust ramps. The massive carbonate formations show bedding-perpendicular stylolites.

[42] The internal deformation features associated with main thrust imbrication are heterogeneously distributed. Thrust surfaces in Marboré sandstone are clean cut, the sandstone layers exhibiting no shear fabric except of closely spaced, transport-perpendicular joints which extend to 1 m from the surface, usually marked by a decimeter thick fault rock composed of thrust-parallel calcite veins. Within the carbonates, there are no signs of strain in the fold backlimbs, while the forelimbs show stylolitic to planar solution cleavage, combined with some homogeneous shortening indicated by strained carbonate nodules or fossils between cleavage planes. Calcite veins, often buckled, are also widespread. The fabric is parallel to fold axial planes, and results in limb thinning. In the weaker shale and turbiditic beds that overlie the carbonates, deformation is expressed by metric-scale chevron folds with slaty cleavage, also restricted to the large-scale forelimb regions.

[43] In addition to this, two sets of subvertical calcite veins parallel to and perpendicular to the transport direction are also widespread in the Aragüés thrust system. Locally these veins are cut by fold-related stylolites. We attribute these veins to extension induced by the load of the overlying thrust sheets. The extension along strike of the imbricates can reach locally up to 5%, although it is heterogeneously distributed in the rock volume.

3.2.5. Significance of Backthrusting

[44] Backthrusts are present in the imbricate pile, in two occurrences: a) at the leading edge of a thrust sheet, defining a frontal box fold (Figure 9d), and b) at the rear of a thrust sheet, over the underlying thrust ramp (Figures 11 and 18). The first type of backthrusts are very common in experimental thrust wedges [*Mulugeta and Koyi*, 1987;

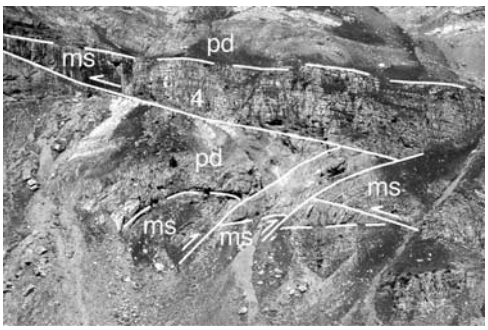

Figure 18. Image of a system of minor backthrusts (dipping left) affecting the Marboré sandstone and the basal tertiary dolomite in the rear of unit 3, just below thrust 4 (see central part of cross section in Figure 11a). The field of view is ~300 m wide, and north is to the right.

Colleta et al., 1991; *Liu et al.*, 1992]. They form early in the propagation history, just ahead of the load of the overlying imbricate. The second type of backthrusts had a different origin: they probably formed at the base of a major thrust ramp due to resistance to motion over the ramp, especially if there was resistance to foreland translation in overlying layers (i.e., Tertiary carbonates). Analogue backthrusts have been obtained in laboratory experiments with small-scale rock models by *Morse* [1977] and *Chester et al.* [1991], and in numerical modeling by *Strayer and Hudleston* [1997].

4. Comparison Between Natural Example and Analogue Models

[45] In the Aragüés field example and the analogue models, layers of different composition had a mechanical significance and accommodated shortening in different ways. The behavior of loose sand in models can be compared to that of the Marboré sandstone, a formation that has higher ductile strength and greater coefficient of internal friction, as suggested by a scarcity of ductile deformation features and by gentle ramp angles. Glass microbead layers can be regarded as a good analogue of the overlying Tertiary carbonates, more prone to ductile deformation.

[46] Modeling sand and Marboré sandstone experienced most shortening by imbrication. In models, this was independent of the stratigraphic position, suggesting that it was not guided by a unidirectional fault propagation from a basal step up in the décollement level. Thin fault zones and gentle cutoff angles in these units passed to more distributed deformation and folding in the weaker carbonates and glass microbeads, defining triangular or funnel-shaped strain zones. The position of these was thus determined by the stratigraphy. In accordance to this, the stratigraphic transitions were accompanied by a marked displacement reduction. Continued displacement variation accumulating after the fault had propagated in the models suggests that changes in the ratio of the resistance to slip to the resistance of folding in compositionally distinct layers may be a mechanism of fault-related folding that may be overlooked in natural thrust-fold structures.

[47] Particular structural geometries as backthrusts at the leading edge fold of a thrust sheet, just in front of the extent of the overlying one, are observed in both experiments and natural example (Figures 3a, 3d, and 9d).

[48] Both the Aragüés system and the sandbox models experienced early layer-parallel shortening, which could not be quantified well in the field example, but accounted for some 20–30% of contraction in the model. Distributed deformation in granular materials was determined by the packing properties (e.g., accommodated by compaction in sand and by layer thickening in glass microbeads). In nature, layer-parallel shortening was also accommodated by different mechanisms according to lithology (minor imbrication, stylolite development, etc.). In spite of different mechanisms, experimental models showed layer-parallel shortening values that did not vary much in different layers. Stratigraphic contrasts have stronger effect on the partition between the other two components of shortening, namely imbrication and folding.

5. Conclusions

[49] In nature and analogue models, mechanical stratigraphy is an important element in the dynamic evolution of foreland thrust systems, as it guides: (1) the partitioning of shortening in different lithologies; (2) thrust faulting styles: changes in fault attitude, ramp angle, displacement, and width of deformation zones along single faults as they cut across different layers; (3) fault-related folding styles: folds are complex and not self-similar in profile, reflecting lithologically controlled variations in propagation, slip and internal deformation rates. These folds do not fit strictly to the classic fault bend or fault propagation models, but are closer to the trishear model. As an alternative to this model, transitions from narrow thrusts to wider, sheared folds occur as the thrust passes through different lithologies (in which the resistance to folding and to fault translation would be different), rather than forming as fault tips propagate in a progressive way through an uniform succession.

[50] Prime factors determining the deformation style in each stratigraphic formation appear to be the relative brittle and ductile strengths, and, to a lesser degree, the layering anisotropy. The results of modeling also indicate that the strength of the décollement level influences the expression of mechanical contrasts between stratigraphic units, where weaker décollements enhance it.

[51] **Acknowledgments.** Thanks are due to J. L. Alonso and P. Labaume for revision of the manuscript. Financial support was provided by projects PB-94-0685 and BTE2000-0159 (CICYT, Spain) and by the Swedish Natural Sciences Research Council (VR).

References

Alonso, J. L., and A. Teixell, Forelimb deformation in some natural examples of fault-propagation folds, in *Thrust Tectonics*, edited by K. R. McClay, pp. 175–180, Chapman and Hall, New York, 1992.

Chester, J. S., Mechanical stratigraphy and fault-fold interaction, Absaroka thrust sheet, Salt River Range, Wyoming, *J. Struct. Geol.*, *25*, 1171–1192, 2003.

Chester, J. S., J. M. Logan, and J. H. Spang, Influence of layering and boundary conditions on fault-bend and fault-propagation folding, *Geol. Soc. Am. Bull.*, *103*, 1059–1072, 1991.

Colleta, B., J. Letouzey, R. Pinedo, J. F. Ballard, and P. Bale, Computerized X ray tomography analysis of sandbox models: Examples of thin-skinned thrust systems, *Geology*, *19*, 1063–1067, 1991.

Davis, D. M., J. Suppe, and F. A. Dahlen, Mechanics of fold-and-thrust belts and accretionary wedges, *J. Geophys. Res.*, *88*, 1153–1172, 1983.

Dixon, J. M., and S. Liu, Centrifuge modelling of the propagation of thrust faults, in *Thrust Tectonics*, edited by K. R. McClay, pp. 53–69, Chapman and Hall, New York, 1992.

Ellis, M. A., and W. J. Dunlap, Displacement variation along thrust faults: Implications for the development of large faults, *J. Struct. Geol.*, *10*, 183–192, 1988.

Erslev, E. A., Trishear fault-propagation folding, *Geology*, *19*, 617–620, 1991.

Gross, M. A., G. Gutiérrez-Alonso, T. Bai, M. A. Wacker, K. B. Collinsworth, and R. J. Behl, Influence of mechanical stratigraphy and kinematics on fault scaling relations, *J. Struct. Geol.*, *19*, 171–183, 1997.

Gutscher, M.-A., N. Kukowski, J. Malavieille, and S. Lallemand, Material transfer in accretionary

wedges from analysis of a systematic series of analog experiments, *J. Struct. Geol.*, *20*, 407–416, 1998.

Hardy, S., and M. Ford, Numerical modeling of trishear fault propagation folding, *Tectonics*, *16*, 841–854, 1997.

Koyi, H. A., Mode of internal deformation in sand wedges, *J. Struct. Geol.*, *17*, 293–300, 1995.

Koyi, H. A., and A. Teixell, Where is the footwall flat? A cautionary note on template constraints, *J. Struct. Geol.*, *21*, 373–377, 1999.

Koyi, H. A., M. Sans, A. Teixell, J. Cotton, and H. Zeyen, The significance of penetrative strain in contractional areas, in *Thrust Tectonics and Petroleum Systems*, edited by K. R. McClay, *Am. Assoc. Petrol. Geol. Mem*., in press, 2003.

Labaume, P., M. Séguret, and C. Seyve, Evolution of a turbiditic foreland basin and analogy with an accretionary prism: Example of the Eocene South-Pyrenean basin, *Tectonics*, *4*, 661–685, 1985.

Liu, H., K. R. McClay, and D. P. Powell, Physical models of thrust wedges, in *Thrust Tectonics*, edited by K. R. McClay, pp. 71–81, Chapman and Hall, New York, 1992.

Liu, S., and J. S. Dixon, Centrifuge modelling of thrust faulting: Strain partitioning and sequence of thrusting in duplex structures, *Geol. Soc. Spec. Publ.*, *54*, 431–444, 1991.

Malavieille, J., Modélisation experimentale des chevauchements imbriquées: Applications aux chaines de montagnes, *Bull. Soc. Geol. Fr.*, *7*, 129–138, 1984.

Marshak, S., and M. S. Wilkerson, Effect of overburden thickness on thrust belt geometry and development, *Tectonics*, *11*, 560–566, 1992.

Mitra, S., Fault-propagation folds: Geometry, kinematic evolution, and hydrocarbon traps, *AAPG Bull.*, *74*, 921–945, 1990.

Morley, C. K., Vertical strain variations in the Osen-Roa thrust sheet, north-western Oslo Fjord, Norway, *J. Struct. Geol.*, *8*, 621–637, 1986.

Morse, J. D., Deformation in ramp regions of overthrust faults: Experiments with small-scale rock models, in *Twenty-Ninth Annual Field Conference*, *Wyoming Geological Association Guidebook*, pp. 457–470, Teton Village, Wyo., 1977.

Mulugeta, G., Modelling the geometry of Coulomb thrust wedges, *J. Struct. Geol.*, *10*, 847–859, 1988.

Mulugeta, G., and H. Koyi, Three-dimensional geometry and kinematics of experimental piggy-back thrusting, *Geology*, *15*, 1052–1056, 1987.

Mulugeta, G., and H. Koyi, Episodic accretion and strain partitioning in a model sand wedge, *Tectonophysics*, *202*, 319–333, 1992.

Mutti, E., The Hecho Eocene submarine fan system, south-central Pyrenees, Spain, *Geo Mar. Lett.*, *3*, 199–202, 1984.

Souquet, P., Le Crétacé supérieur sudpyrénéen en Catalogne, Aragon et Navarre, thèse d'etat, Univ. é Paul Sabatier, Toulouse, France, 1967.

Storti, F., F. Salvini, and K. R. McClay, Fault-related folding ind sandbox analogue models of thrust wedges, *J. Struct. Geol.*, *19*, 583–602, 1997.

Strayer, L. M., and P. J. Hudleston, Numerical modelling of fold initiation at thrust ramps, *J. Struct. Geol.*, *19*, 551–566, 1997.

Suppe, J., Geometry and kinematics of fault-bend folding, *Am. J. Sci.*, *283*, 684–721, 1983.

Suppe, J., and D. A. Medwedeff, Geometry and kinematics of fault-propagation folding, *Eclogae Geol. Helv.*, *83*, 409–454, 1990.

Teixell, A., Alpine thrusts at the western termination of the Pyrenean Axial zone, *Bull. Soc. Geol. Fr.*, *8*, 241–249, 1990.

Teixell, A., The Ansó transect of the southern Pyrenees: Basement and cover thrust geometries, *J. Geol. Soc. London*, *153*, 301–310, 1996.

Turrini, C., A. Ravaglia, and C. R. Perotti, Compressional structures in a multi-layered mechanical stratigraphy: Insights from sandbox modeling with three-dimensional variation in basal geometry and friction, *Geol. Soc. Am. Mem.*, *193*, 153–178, 2001.

Van Elsberg, J. N., Geology of the upper Cretaceous and part of the lower Tertiary, north of Hecho and Aragüés del Puerto (Spanish Pyrenees, province of Huesca), *Estud. Geol.*, *24*, 39–77, 1968.

Woodward, N. B., and E. Rutherford, Structural lithic units in external orogenic zones, *Tectonophysics*, *158*, 247–267, 1989.

H. A. Koyi, Hans Ramberg Tectonic Laboratory, Department of Earth Sciences, Uppsala University, Villavagen 16, 752 36 Uppsala, Sweden. (hemin.koyi@geo.uu.se)

A. Teixell, Departament de Geologia, Universitat Autònoma de Barcelona, E-08193 Bellaterra, Spain. (antonio.teixell@uab.es)


(a)
1
2
3
4
5
(b)
3
4
5
(c)
4
(d)
3

Figure 9. (opposite) Field photographs of the Aragüés thrust system. (a) Panoramic view of the Osia valley and the entire thrust system from the southwest. (b) Photograph looking east of the northern part of the system. The Marboré sandstone appears brown-weathered in the center and left, whereas the white cliffs correspond to the Tertiary carbonates. The slope is ~500 m high. Compare with the cross section of Figure 11b. (c) Ramp of thrust 4 in the eastern side of the valley. The Marboré sandstone is in the nearest hanging wall (brown), and the Paleocene dolomite (grey) and massive limestone (white) are in the footwall. The image is ~250 m wide. (d) Frontal box fold at the leading edge of thrust unit 3, very similar to those obtained in analogue models. The field of view is ~500 m wide, and north is to the left. The Marboré sandstone (lower left) shows a gentle cutoff angle; the poorly exposed unit is the massive dolomite, and the overlying limestone units show a overturned box fold with marked forelimb thinning.